remote sensing

MDPI

Article

Lidar-Imagery Fusion Reveals Rapid Coastal Forest Loss in Delaware Bay Consistent with Marsh Migration

Elisabeth B. Powell [1,*], Kari A. St. Laurent [2] and Ralph Dubayah [1]

[1] Geographic Sciences Department, University of Maryland, 2181 LeFrak Hall, College Park, MD 20742, USA
[2] Delaware Department of Natural Resources and Environmental Control, Delaware National Estuarine Research Reserve, Dover, DE 19734, USA
* Correspondence: epowell1@terpmail.umd.edu

Abstract: Tidal wetland ecosystems and their vegetation communities are broadly controlled by tidal range and inundation frequency. Sea-level rise combined with episodic flooding events are causing shifts in thresholds of vegetation species which reconstructs the plant zonation of the coastal landscape. More frequent inundation events in the upland forest are causing the forest to convert into tidal marshes, and what is left behind are swaths of dead-standing trees along the marsh–forest boundary. Upland forest dieback has been well documented in the mid-Atlantic; however, reliable methods to accurately identify this dieback over large scales are still being developed. Here, we use multitemporal Lidar and imagery from the National Agricultural Imagery Program to classify areas of forest loss in the coastal regions of Delaware. We found that 1197 ± 405 hectares of forest transitioned to non-forest over nine years, and these losses were likely driven by major coastal storms and severe drought during the study period. In addition, we report decreases in Lidar-derived canopy height in forest loss areas, suggesting forest structure changes associated with the conversion from forest to marsh. Our results highlight the potential value of integrating Lidar-derived metrics to determine specific forest characteristics that may help predict future marsh migration pathways.

Keywords: remote sensing; marsh migration; ghost forest; change detection; Lidar; forest structure

check for updates

Citation: Powell, E.B.; Laurent, K.A.S.; Dubayah, R. Lidar-Imagery Fusion Reveals Rapid Coastal Forest Loss in Delaware Bay Consistent with Marsh Migration. *Remote Sens.* **2022**, *14*, 4577. https://doi.org/10.3390/rs14184577

Academic Editor: Andrea Nascetti

Received: 20 July 2022
Accepted: 9 September 2022
Published: 13 September 2022

Publisher's Note: MDPI stays neutral with regard to jurisdictional claims in published maps and institutional affiliations.

Copyright: © 2022 by the authors. Licensee MDPI, Basel, Switzerland. This article is an open access article distributed under the terms and conditions of the Creative Commons Attribution (CC BY) license (https://creativecommons.org/licenses/by/4.0/).

1. Introduction

Coastal wetlands provide crucial ecosystem services, with these landscapes acting as nekton nurseries, providing wave attenuation, absorbing carbon, and improving water quality by sequestering and removing excess nutrients [1,2]. Coastal wetlands must vertically gain elevation (sediment accretion) at rates greater than or equal to sea-level rise (SLR) to resist converting to mudflats or open water. Yet, it is unclear if coastal marshes will be able to keep up with the current pace of SLR, especially in the mid-Atlantic, where SLR rates are three to four times higher than global averages [3].

Accelerated SLR threatens coastal landscapes as the vegetation community has varying tolerances to increased inundation and salinity [4]. The vegetation of the estuarine landscape is unique as individual plant species are adapted to live in areas with specific salinity and moisture regimes controlled by the influx of tides and groundwater [5]. Therefore, increased inundation and saltwater intrusion from SLR can shift the thresholds of vegetation species, leading to the reconstruction of plant zonation of the coastal landscape [6–9] (Figure 1). Marsh vertical accretion rates less than SLR can cause these ecosystems to convert to open water (i.e., marsh drowning); however, marsh vegetation can migrate upslope into the upland forest to resist conversion [10–12]. This conversion from upland forest to tidal marsh is termed "marsh migration" and may offset marsh loss caused by erosion at the seaward edge [8,9,13].

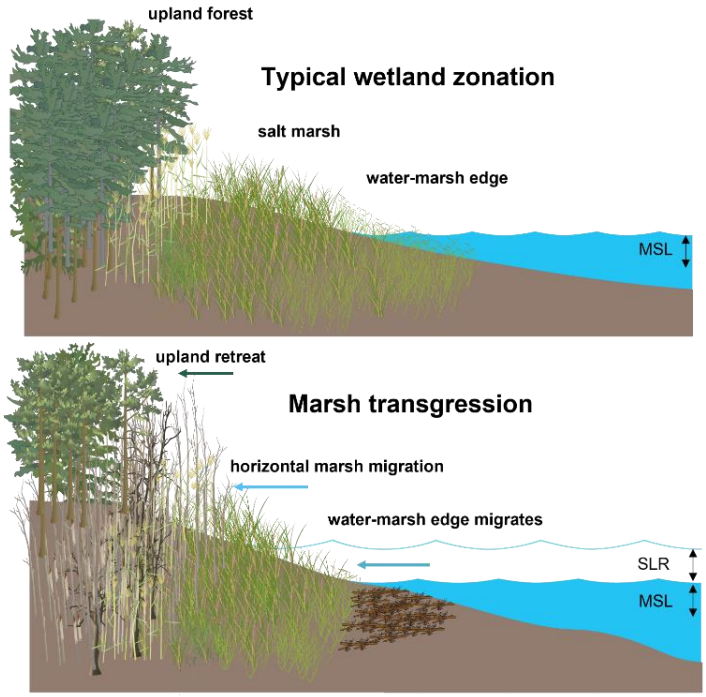

Figure 1. Conceptual diagram of the typical wetland zonation (**top panel**) and ecosystem responses to SLR (**bottom panel**). SLR causes shifts in thresholds of vegetation species, causing reconstruction of the plant zonation of the coastal landscape, leading to marsh transgression (diagram modified from ian.umces.edu/media-library).

As the upland forest becomes increasingly exposed to inundation and salinity with gradual SLR, changes to the edaphic characteristics inhibit regeneration and ultimately lead to mature tree death [9,11,14]. The subsequent and successive forest dieback and the lack of regeneration of new trees increase light exposure, allowing salt-tolerant halophytic plants to colonize the formerly forested area. As upland forests are converted into a marsh, what remains are standing tree snags and stumps surrounded by marsh vegetation often termed '*ghost forests*' [4,12,15].

Rapid conversion from forest to marsh and the development of ghost forests can also occur following an intense storm. Accelerated SLR and coastal storms are inherently linked, as storms' flooding frequency dramatically increases with higher sea levels [11,12,16]. Additionally, global warming is likely to intensify and increase the frequency of coastal cyclones in the North Atlantic ocean, compounding the effects of SLR-induced flooding on coastal landscapes [17]. Strong winds and storm surges produced by coastal storms can cause rapid forest dieback. Strong winds damage the physical forest structure, leading to canopy defoliation and tree uprooting, whereas prolonged flooding from intensified storm surges starves the soil of oxygen and promotes the activity of sulfide-producing bacteria, creating a toxic environment for upland plants [11,18–20]. Additionally, increased soil salinity can lead to canopy browning, defoliation, alter freshwater uptake by roots, and inhibit forest regeneration [19,21–23]. Forest dieback and lack of forest regeneration from episodic events can facilitate rapid marsh migration as short-term forest recovery may not be possible, leading to the transition from forest to marsh over much shorter time scales. Moreover, forest dieback triggered by a strong storm may pave the way for further upslope marsh expansion as the forest seedlings may be more sensitive to the effects of gradual SLR, thereby shifting the regeneration niche further inland [9].

In contrast to the landscape effects of increased tidal flooding, upland environments can also be converted into marshes from saltwater intrusion into the groundwater. Although linked with gradual SLR, the result of saltwater intrusion on upland habitats may precede the effects of increased tidal inundation [24].

Marsh migration may be the most salient process for estimating future wetland resiliency to accelerated SLR and frequency in coastal storms. Recent evidence has suggested that global wetlands' resiliency primarily depends on the availability of accommodation space or adequate lateral space for wetlands to colonize and persist with SLR [25,26]. However, the timing and process by which the marsh vegetation replaces upland vegetation are poorly understood, as many factors influence the ability for upslope migration and future resiliency to SLR (e.g., sediment supply, accretion rates, topography, management, land use, and hydrology) [11,12,26].

Evidence supports that upland forest dieback driven by accelerated SLR may vary over spatial scales as specific site conditions could influence various magnitudes of forest dieback; however, there is limited literature using remote sensing to understand large scale coastal forest decline and its mirror image–inland marsh migration [3,10,26,27]. Previous work has focused on measuring upslope marsh expansion and subsequent forest dieback over time using historical aerial photographs and other optical sensors [4,27–29]. While this approach helps trace the landward migration of marshes into forests that have been defoliated, more subtle changes to the forest structure, such as loss in canopy height, could be early signs of initial marsh expansion before extensive forest dieback occurs.

Forest structure changes can be observed using Lidar remote sensing [30,31]. The height of the vegetation can act as an indicator for species composition, successional stage, climate, and land cover classification [30]. Furthermore, the combination of high-resolution Lidar data and high-resolution aerial imagery may be a powerful tool to classify and monitor changes associated with marsh migration [32]. This combination results in better classification accuracy than with imagery alone [32]. For example, Smart et al. [3] used multitemporal Lidar and spectral indices derived from Landsat to map ghost forests along the Albemarle-Pamlico Peninsula in North Carolina; however, the multi-temporal Lidar was resampled to match the resolution associated with Landsat (30-m). This coarser resolution may miss areas experiencing initial dieback along the upland-marsh boundary, especially in areas where the widths of forests adjacent to tidal wetlands are thin. Thus, there is considerable interest in exploring the potential of high-resolution Lidar and imagery toward detecting changes in forest structure as an indicator for future marsh migration.

In this paper, we quantify recent coastal forest loss between 2007 to 2015 in the coastal areas in Delaware using multi-temporal high-resolution imagery from the National Agriculture Imagery Program (NAIP) and publicly available airborne Lidar. The remainder of this paper is as follows: we first discuss the data and methodology used for the change detection, then report the area of recent forest loss and investigate larger landscape patterns and potential predictors for forest loss within the local 12-Hydrologic Unit Code (HUC-12) watersheds. We further explore the utility of airborne Lidar to observe changes to canopy height that may be associated with forest structure changes ensued by marsh migration. Finally, we discuss relevant environmental drivers that may have induced the rapid conversion of forest to marsh over this sub-decadal timespan.

2. Materials and Methods

2.1. Study Area

Areas along Delaware Bay are some of the lowest-lying areas in the US and thus are at risk for SLR-induced flooding impacts. The vegetation along Delaware Bay is adapted to a range of salinities, including tidal freshwater, brackish, and salt marshes. The different wetland types are associated with slight differences in elevation and the flooding regime [21]. The coastal areas of New Castle and Kent Counties in Delaware are the main focus areas for our study (Figure 2).

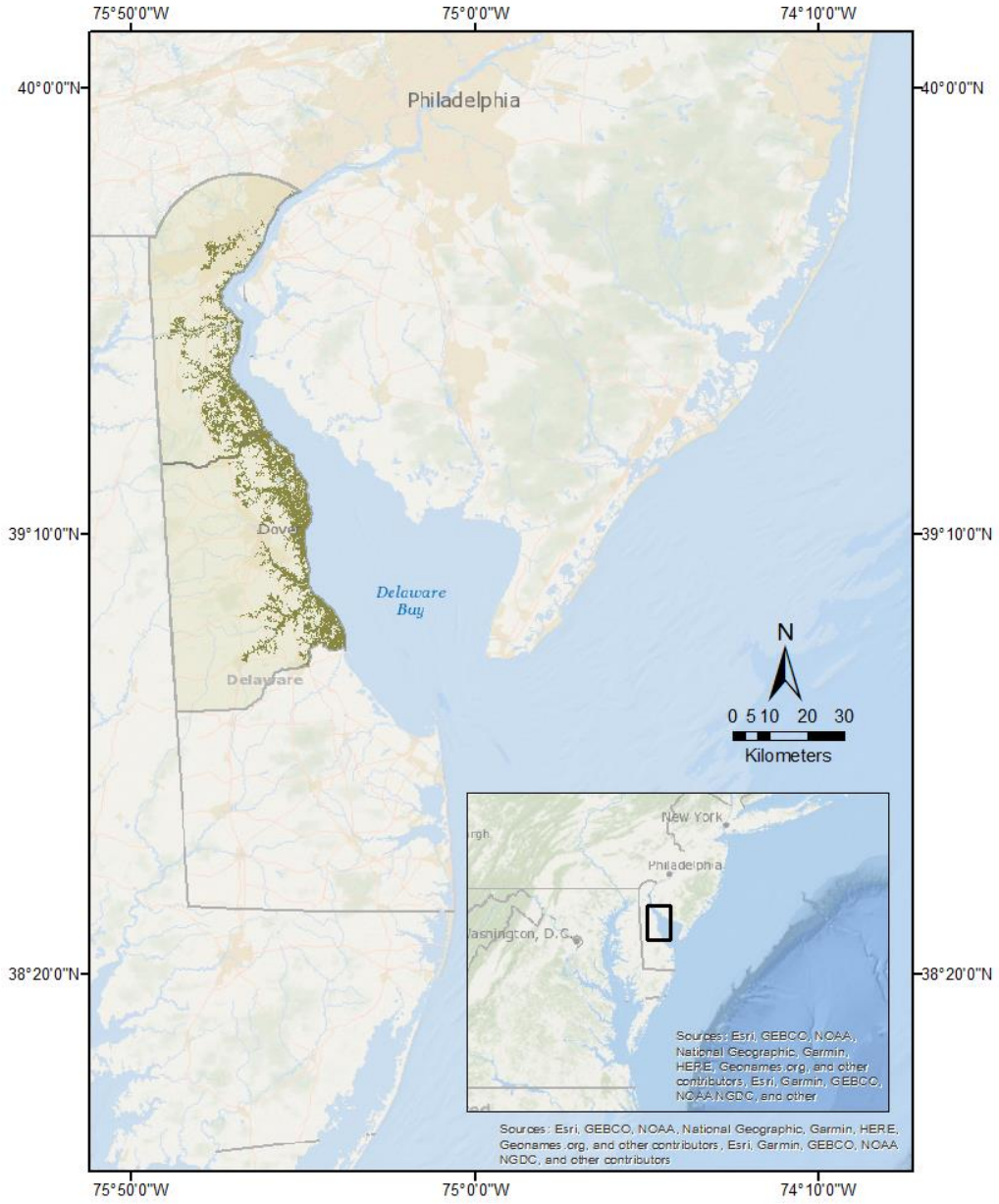

Figure 2. Map of the study area, coastal areas of New Castle and Kent Counties Delaware.

In Delaware Bay, *Spartina alterniflora* (Smooth Cordgrass) occurs at the estuary's lowest elevations, where tidal-driven saltwater flooding occurs twice daily. Vegetation in higher elevations that are inundated only during spring tides is comprised of a mix of grasses, including *Spartina patens* (Salt Hay), *Distichlis spicata* (Desert Saltgrass), and *Juncus gerardii* (Blackgrass). The upland edge, where inundation is increasingly occurring with SLR, is commonly colonized by *Phragmites australis*, marsh elder (*Iva frutenscens*), and eastern red cedar (*Juniperus virginiana*) [33].

The upland forests in the study area are comprised of deciduous hardwoods and evergreens, where forest composition shifts as the soil saturation increases [33,34]. Drier upland forests consist of several Oaks (e.g., white (*Quercus alba*), southern red (*Q. falcata*), scarlet (*Q. coccinea*), black (*Q. velutina*)) and Pines (e.g., pitch (*Pinus rigida*), loblolly (*P. taeda*), and Virginia (*P. virginiana*) and shortleaf (*P. echinata*)) [33,34]. In areas with higher soil saturation, the forest tends to be made up of red maple (*Acer rubrum*), black gum (*Nyssa sylvatica*), American Holly (*Ilex opaca*), and Atlantic White Cedar (*Chamaecyparis thyoides*) [33,34].

Our study areas were classified as 'estuarine and marine wetlands', 'freshwater emergent wetlands' and 'freshwater forested/shrub wetlands', identified by the 2020 National Wetland Inventory (NWI). We also included the adjacent forest within 75 m of wetland areas as we are interested in the upslope retreat of the forest further inland, and these extents may not be classified as freshwater forested/shrub wetlands by the NWI [35].

2.2. Remote Sensing Data

2.2.1. Airborne Lidar Data

The raw point clouds for each year were downloaded from the NOAA Digital Coast Data viewer [35]. All Lidar processing was performed using the lidR package [36] in the R computing environment (R Core Team 2020, Vienna, Austria). The 2014 Lidar acquisition had an average point density of 4.1 points/m^2, while the 2007 acquisition had an average point density of 1.3 points/m^2 (Table 1). To allow for proper comparison between the two Lidar acquisitions, the point densities for the two acquisitions were reduced to 1 point/m^2 using the *lasfilterdeciminate* function in the lidR package, which randomly removes a given proportion of points to achieve a specific point density [36,37]. After attaining the proper point density, the point clouds were filtered of noise and duplicate points and then normalized into height above the ground or a normalized Digital Surface Model (nDSM) with a 2-m horizontal resolution using linear interpolation. A 2-m digital elevation model (DEM) was also generated with ground points using Delaunay triangulation. Using the local maximum of the nDSM, we determined the height of the canopy and derived a 2-m resolution canopy height model (CHM). Additionally, the standard deviation of the normalized heights within a 2-m cell was generated and gridded into a raster.

Table 1. Airborne LiDAR flight acquisition details for 2007 and 2014, acquired from the Sanborn Map Company, Inc and NOAA National Geodetic Survey, respectively.

Year	Instrument	Flight Altitude (m AGL)	Scan Frequency (Hz)	Pulse Rate (kHz)	Scan Angle	Point Density (Points/m^2)
2007	Leica Systems ALS-50	1400	32	50	20	4.1
2014	Leica Systems ALS-70	1676	31.7	165	17	1.3

2.2.2. NAIP Imagery

The NAIP imagery was acquired and mosaicked as one single image for each county for each year [38]. Leaf on, 1-m resolution 4-band NAIP imagery was only available for 2009 and 2015. Despite the temporal mismatch of the Lidar and NAIP imagery acquisitions, we do not expect high temporal discrepancies as there were no instances of fire or severe storms that would produce major height changes between 2007–2009 and 2014–2015 [39]. The composites of the NAIP imagery included the visible spectrum (red, green, blue, RGB) and the near-infrared (NIR) band. From the imagery composite, we calculated the normalized difference vegetation index (NDVI).

Additionally, a Principal Component Analysis (PCA) was carried out on the NAIP to minimize spectral redundancy. The NAIP imagery was resampled to 2-m resolution by nearest-neighbor interpolation in ArcGIS 10.6 software to match the derived Lidar gridded products. Finally, the resampled NAIP imagery and PCA layers were clipped to the tidal wetlands and adjacent forest areas.

2.3. Random Forest Classification

We used the randomForest [40] and caret [41] packages in R statistical software (RStudio, Inc. Boston, MA, USA, v1.3.1073). Tuning in caret was applied using the tuneRF function to determine the hyperparameters for the RF classifier. Once these were found, we used 10-fold cross-validation and three repeats to limit and reduce overfitting [42].

The training dataset for the RF was derived from the raw high-resolution (1-m) leaf-on NAIP imagery. We manually classified 1500 points as 'forest' or 'non-forest' using expert knowledge, of which, 80% were used for training and 20% were withheld for testing [42]. Forest areas were identified when a canopy was present, while non-forest points were identified when no canopy was present. Non-forest points were dominated by marsh grasses, bare ground, and open water but because we focused on changes to the forest from recent marsh migration, classifying other vegetation zones within the 'non-forest' was not a priority as wetland vegetation zones are highly heterogeneous and subject to misclassification from visual interpretation.

Once the best parameters for the RF classifier were found, the model was evaluated against the test data, and model accuracy was assessed using the built-in random forest confusion matrix function. Additionally, variable importance was analyzed using the Mean Decrease in Accuracy (MDA) [43]. The MDA compares the Out-of-Bag (OOB) error through random permutations of the values of different variables and the OOB error from the original data set [43]. More simply, the MDA is the decrease in prediction accuracy relative to the original model when a variable is removed.

Once the random forest classifier was appropriately trained and tuned, it was applied to each year's stacked Lidar and NAIP imagery. For simplification, the resulting forest/non-forest map classified with the 2007 Lidar/2009 NAIP imagery is referred to as the 2009 forest/non-forest classification map, whereas the resulting forest/non-forest map classified with the 2014 Lidar and 2015 NAIP imagery is referred to as the 2015 forest/non-forest classification map.

2.4. Change Map and Accuracy Assessment

Although the accuracies of classifications from the two dates may be high, the derived change map can be inaccurate, and the area computed by the change map may be biased [40], as traditional pixel counting can be unreliable in calculating the actual proportion of classified areas [44,45]. Using a sample-based estimator to assess the accuracy of the change map, we can avoid the measurement bias of pixel counting and decrease the standard error of the area estimate [44]. The stratified estimator method is viewed as an "error-adjusted" estimation of the area because it includes the erroneous map area associated with the omission error and omits the area related to the commission error [44].

The equations detailed in Olofsson et al. [44] were used to determine the estimated error with each *from-to* transition with the associated 95% confidence interval. The samples used for the accuracy assessment of the change map were independent of the training dataset used in the RF classification. The reference land cover of each sample was determined using the raw high-resolution NAIP imagery (1-m). The error matrix consisted of sample counts with map categories as rows and reference categories as columns. Class 1 was no change to non-forest (non-forest stable), class 2 was forest to non-forest (forest loss), class 3 was non-forest to forest (forest growth), and class 4 was no change to forest (stable forest). User's, Producer's, and overall accuracy were calculated based on the error matrix. In addition, the change classes' area was updated with the accuracy assessment findings using the stratified estimation method [44,46].

2.5. Landscape Change Analysis

Forest to non-forest vegetation transition areas were tabulated for the study area's HUC-12 watersheds to investigate larger landscape patterns in upland forest loss and to analyze the predictive power of hydrologic connectivity and elevation to explain increased forest losses. The tabulated area of the forest losses was normalized by dividing by the classified forest area in the 2009 forest map in each HUC to account for differences in forest extents.

Drainage maps were derived from the United States Geologic Survey (USGS) National Hydrography Dataset (NHD) downloaded from Delaware First Map [47]. We calculated the drainage density of each subregion following the methods of White et al. [27] by

dividing the total length of the drainage features (artificial, canal/ditch, river/stream) by the total subregion area. These hydrologic features included river channels, tidal creeks, and artificial ditches. Additionally, the average elevation of each HUC was derived from the 2014 digital elevation model. Finally, Spearman correlation compared drainage density and average elevation to the normalized tabulated area of forest to non-forest.

We extracted the canopy height (greater than 1 m) and ground elevation from the 2007 and 2014 Lidar in areas with classified forest loss, forest growth, and stable forest to explore whether the canopy height and elevation change were directionality positive or negative between the change classes. Additionally, a height transition matrix was constructed to determine the probability of height changes over seven years [48,49]. Height transition matrices characterize forest dynamics and incorporate growth and lateral filling, death and branch loss [48]. For this matrix, all canopy heights were binned into 2-m vertical intervals but were limited to forested areas identified by NWI and the Delaware Canopy Cover map [50]. The matrix columns report the likelihood of a height transitioning from a 2007 height class to a 2014 height class while reading across the rows gives a chance that the observed height in 2014 originated from the height class in 2007 [48,49].

3. Results

3.1. Classification and Change Map Results

The RF classifiers performed with high accuracies, and the Lidar-derived metrics slightly enhanced classification accuracy compared to using imagery alone. The overall accuracy of the two forest/non-forest classification maps for 2009/2015 was 93% and 91%, respectively, whereas, without the Lidar metrics, accuracy was 87% and 86%. The change map produced by the post-classification comparison of the 2009 and 2015 forest/non-forest classification maps had an overall accuracy of 91% (Figure 3a) (Table 2).

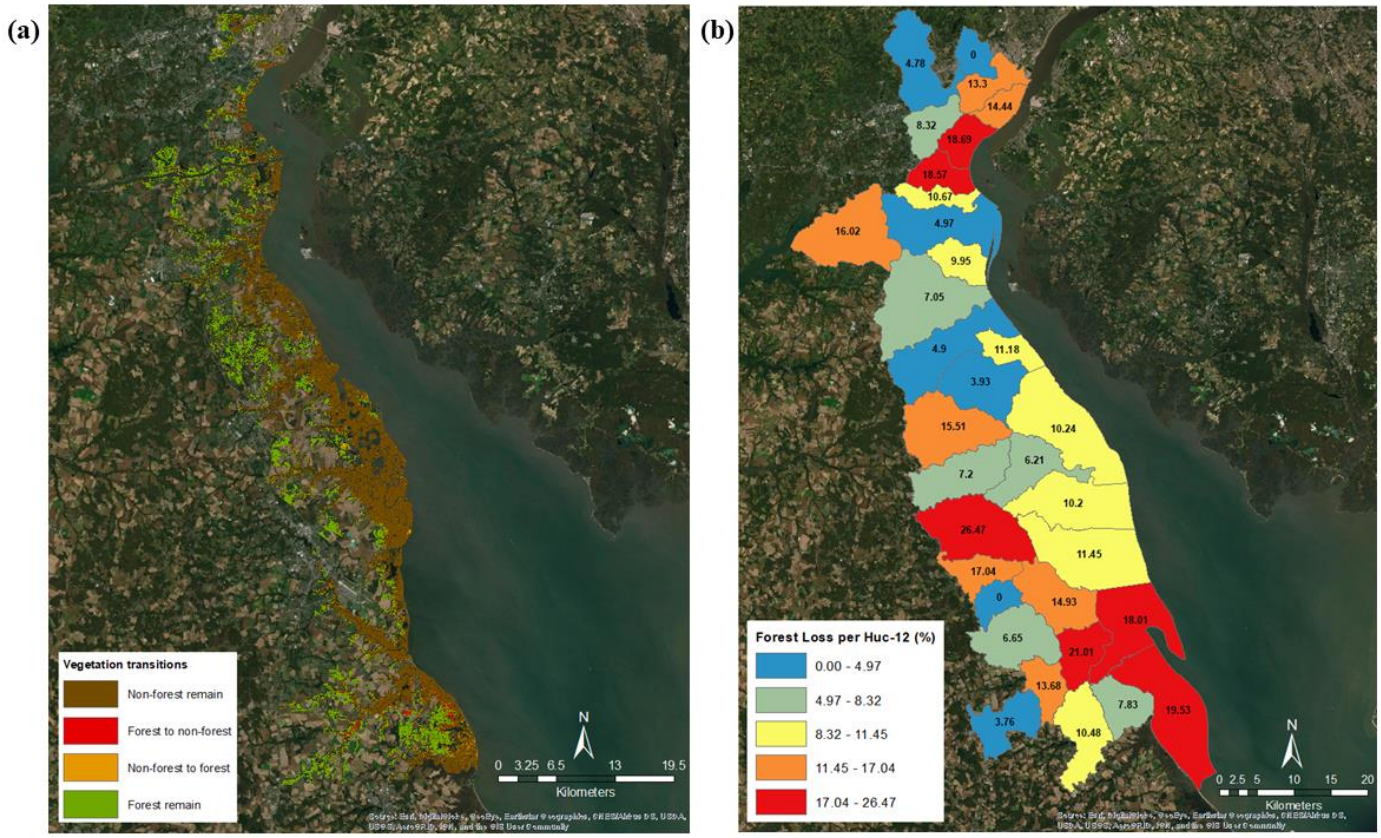

Figure 3. Change map of the study area from the post-classification analysis (**a**). Normalized area of forest loss per HUC 12 hydrologic subregion (**b**).

Table 2. Accuracy assessment of the change map error matrix. Class 1 is no change to non-forest areas, class 2 is forest to non-forest transition, class 3 is non-forest to forest transition, and class 4 is no change to forest areas. W_i is the proportion of the area that is mapped to a specific class divided by the total mapped area. Map categories are the rows, while reference categories are the columns.

Class	1	2	3	4	Total	Map Area (ha)	W_i	Users	Producers	Overall
1	193	2	1	4	200	19,098	0.58	0.97	0.95	0.91
2	45	98	0	57	200	1216	0.04	0.49	0.50	
3	107	3	9	81	200	1149	0.04	0.05	0.35	
4	3	7	0	190	200	11,252	0.34	0.95	0.90	
Total	348	110	10	332	800	**32,715**				

A major research objective of this study was to quantify upland forest dieback that may be associated with recent routes of marsh migration; therefore, the accuracy of the transition from forest to non-forest is of particular interest. Using the pixel count method, the area calculated from the change map for the forest to non-forest transition (forest loss) was 1217 ha.

This area falls within the 95% confidence interval of the error-adjusted estimated area (1197 ± 405 ha). This error-adjusted area is less than the pixel count, as the commission error was prominent in the change accuracy assessment (Table 3) [44].

Table 3. Land transition area (hectares) for each change class using the pixel count and error-adjusted area methods. The equations detailed in Olofsson et al. [42] were used to determine the estimated error with each from–to transition with the associated 95% confidence interval.

Area Calculation Method	Land Transition (ha)			
	Non-Forest Remain	Forest to Non-Forest	Non-Forest to Forest	Forest Remain
Pixel count	19,098	1217	1149	11,252
Error adjusted area	19,486 ± 708	1197 ± 405	147 ± 32	11,882 ± 806

The area of the non-forest to forest (forest growth) change class derived by pixel count was well outside the bounds of the error-adjusted area (147 ± 32 ha). Errors of commission dominated this change class, which reflects the reduced area. The areas calculated by pixel count for the stable change classes (no change to forest, no change to non-forest) were within the error-adjusted area confidence intervals (Table 3).

We found that approximately 4.1% of the total classified area transitioned to a new vegetation class during the study period. However, the non-forest to forest transition (forest-growth) class was prone to commission errors. This may be due to the classifier's confusion with the heterogeneous wetland vegetation along the upland-marsh transitional ecotone, which we will discuss later.

3.2. Landscape Change Analysis

The normalized area of forest loss within each HUC-12 subregion was not associated with any specific spatial gradient, but higher percentages of losses were concentrated further south in the estuary (Figure 3b). The Upper Saint Jones River subregion accounts for the highest rates of forest losses, accounting for 26% of the forest classified in the 2009 forest map, which converted to non-forest.

Drainage density was somewhat correlated ($R = -0.37$, $p = 0.049$) with the percentage of forest loss in each HUC-12 subregion. Our analysis suggests that watersheds with higher drainage densities are less likely to experience forest dieback than subregions with lower drainage densities (Figure 4). We did not find a significant relationship between mean elevation and tabulated forest loss.

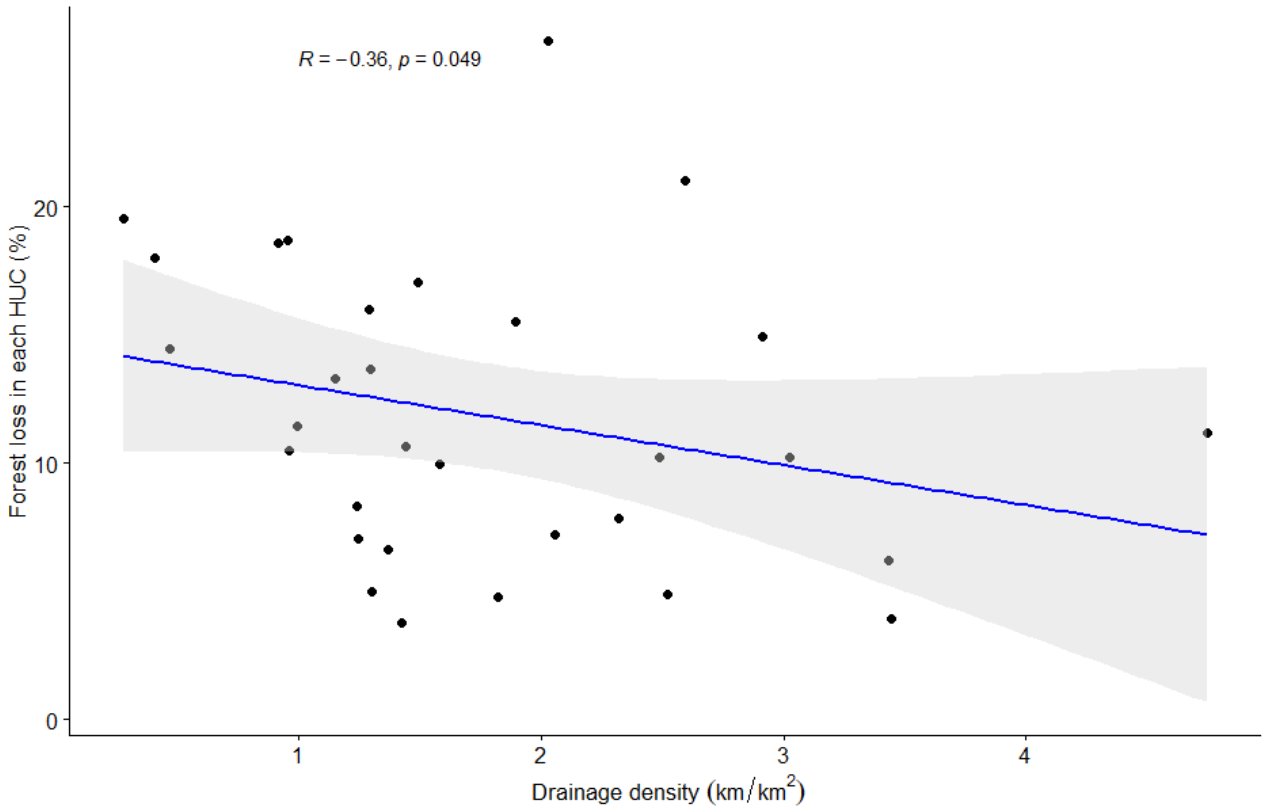

Figure 4. Spearman correlation of percentage of forest loss per HUC (%) and drainage density.

The canopy height in areas that transitioned from forest to non-forest decreased from 2007 to 2014 (Figure 5). In 2007, the mean canopy height in areas with forest loss was 11.97 ± 6.50 (SD) meters, whereas, in 2014, the canopy height was 10.79 ± 7.24, identifying overall reductions in tree height during the study period (Table 4). In contrast, in areas classified as forest remaining (forest stable) and forest growth (non-forest to forest), canopy heights increased from 2007 to 2014. In areas with stable forests (no change to forest), the mean canopy height in 2007 was 16.89 ± 6.91 m and 17.81 ± 7.08 m in 2014. In areas classified with forest growth, the mean canopy height was 7.59 ± 6.15 m in 2007 and 9.73 ± 5.91 in 2014 (Table 4).

Table 4. Summary statistics of multi-temporal canopy height and ground elevation among the change classes.

	2007 Canopy Height (m)			**2014 Canopy Height (m)**			
	Mean	**Median**	**sd**	**Mean**	**Median**	**sd**	**n**
Forest loss	11.97	11.40	6.50	10.79	9.57	7.24	1,496,807
Forest remain	16.89	17.26	6.91	17.81	18.28	7.08	25,653,049
Forest growth	7.59	5.43	6.15	9.73	8.61	5.91	674,500
	2007 Ground Elevation (m)			**2014 Ground Elevation (m)**			
	Mean	**Median**	**sd**	**Mean**	**Median**	**sd**	**n**
Forest loss	2.99	1.31	3.92	2.96	1.28	3.91	1,496,807
Forest remain	6.29	4.49	5.44	6.29	4.51	5.43	25,653,049
Forest growth	3.19	1.09	4.93	3.17	1.10	4.90	674,500

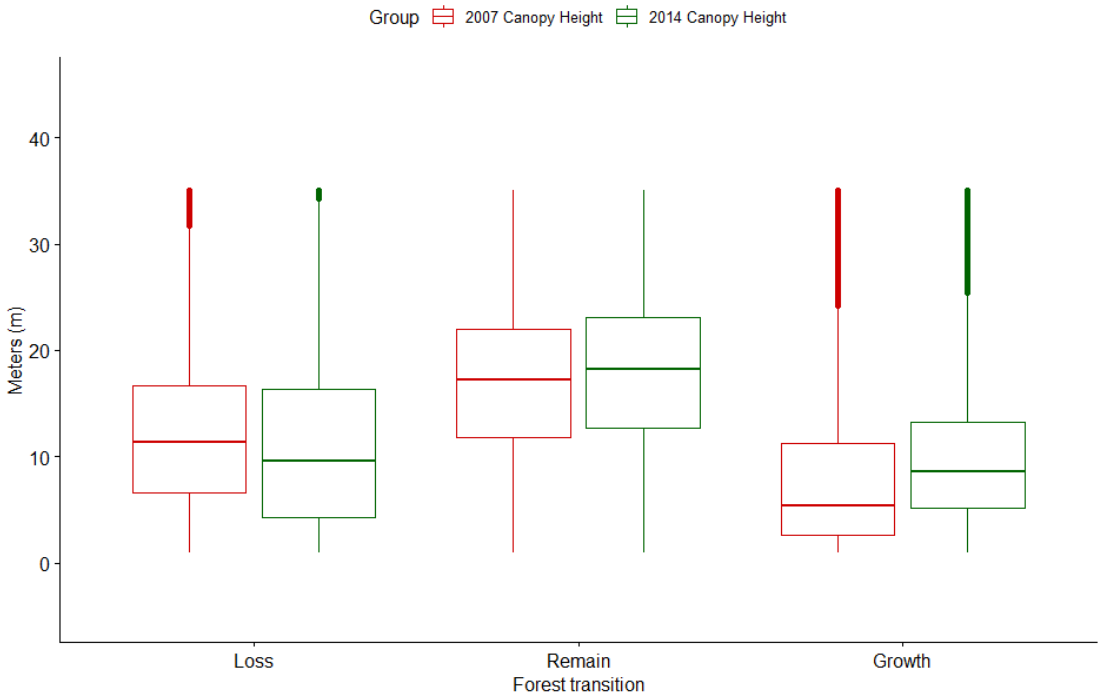

Figure 5. Comparison of canopy height from 2007 and 2014 across the forest transition classes.

Ground elevations varied across the forest transition classes and appeared to be lowest in forest loss areas compared to stable forest and growth areas. Overall, ground elevation appeared to remain stable within the change classes, with slight decreases from 2007 to 2014 in areas of forest loss, which may have resulted from the subsequent subsidence following forest dieback due to marsh migration (Figure 6).

Generally, the diagonal of the transition matrix follows an increasing trend following the 8–10 m height class, indicating that the taller canopy heights in 2007 were less likely to transition to a new height class (Table 5). On the other hand, heights in-between 2 and 8 m display an overall decreasing trend in the diagonal, identifying increased chances to transition into new height classes. These transition likelihoods for heights between 2 and 8 m are weighted toward height gains compared to losses. However, these gains do not necessarily require that the vertical growth of the canopy grows but can also occur as adjacent canopy gaps and overhead are latterly filled. These transition probabilities are consistent with the average canopy heights in upland dieback and stable forest areas, where we see higher probabilities of transitioning to a new height class when heights are lower than 12 m and greater chances of height stability in regions with taller canopy heights (Table 4).

Our data show conversion probabilities to the shortest height class (<2 m) in 2014 from taller height classes in 2007 across all the classes (including tallest) (see the first row of Table 5), demonstrating cases of tree mortality for all height classes over the seven years. This transition accounts for almost ~7% of the total Lidar footprints, suggesting widespread height loss. These losses may not be the overall vertical tree height reduction but rather enough branch death to produce a gap that extends through the canopy and remains in 2014. We speculate that these canopy gaps may represent the widespread thinning of the forest canopy due to edaphic stress related to prolonged inundation events.

Table 5. Matrix of height transitions from 2007 to 2014.

	2007 Height																			
2014 Height	**<2**	**2–4**	**4–6**	**6–8**	**8–10**	**10–12**	**12–14**	**14–16**	**16–18**	**18–20**	**20–22**	**22–24**	**24–26**	**26–28**	**28–30**	**30–32**	**32–34**	**34–36**	**>36**	**N**
<2	**0.37**	0.16	0.13	0.12	0.10	0.09	0.08	0.07	0.07	0.06	0.06	0.06	0.06	0.06	0.06	0.07	0.08	0.08	0.08	4344354
2–4	0.15	**0.20**	0.08	0.05	0.04	0.03	0.02	0.02	0.02	0.01	0.01	0.01	0.01	0.01	0.01	0.01	0.01	0.01	0.01	1635554
4–6	0.13	0.20	**0.17**	0.07	0.04	0.03	0.02	0.02	0.01	0.01	0.01	0.01	0.01	0.01	0.01	0.01	0.01	0.01	0.01	1710029
6–8	0.10	0.15	0.19	**0.17**	0.07	0.04	0.03	0.02	0.01	0.01	0.01	0.01	0.01	0.01	0.01	0.01	0.01	0.01	0.01	1840462
8–10	0.07	0.11	0.16	0.20	**0.17**	0.07	0.04	0.03	0.02	0.01	0.01	0.01	0.01	0.01	0.01	0.01	0.01	0.01	0.01	2050641
10–12	0.05	0.07	0.11	0.16	0.21	**0.18**	0.07	0.04	0.02	0.02	0.01	0.01	0.01	0.01	0.01	0.01	0.01	0.01	0.00	2311029
12–14	0.03	0.04	0.06	0.11	0.16	0.22	**0.19**	0.07	0.04	0.02	0.02	0.01	0.01	0.01	0.01	0.01	0.01	0.00	0.00	2580172
14–16	0.03	0.02	0.03	0.05	0.09	0.16	0.24	**0.21**	0.08	0.04	0.02	0.02	0.01	0.01	0.01	0.01	0.01	0.01	0.00	2828951
16–18	0.02	0.02	0.02	0.03	0.05	0.09	0.16	0.25	**0.22**	0.08	0.04	0.02	0.02	0.01	0.01	0.01	0.01	0.01	0.01	3037465
18–20	0.02	0.01	0.02	0.02	0.03	0.04	0.08	0.16	0.27	**0.23**	0.08	0.04	0.03	0.02	0.01	0.01	0.01	0.01	0.00	3180714
20–22	0.01	0.01	0.01	0.01	0.02	0.02	0.04	0.07	0.15	0.29	**0.25**	0.09	0.04	0.03	0.02	0.02	0.01	0.01	0.01	3197649
22–24	0.01	0.01	0.01	0.01	0.01	0.01	0.02	0.03	0.06	0.14	0.30	**0.27**	0.09	0.05	0.03	0.02	0.02	0.01	0.01	3008949
24–26	0.01	0.00	0.01	0.01	0.01	0.01	0.01	0.01	0.02	0.05	0.13	0.31	**0.29**	0.10	0.05	0.03	0.02	0.02	0.01	2522858
26–28	0.01	0.00	0.00	0.00	0.00	0.00	0.00	0.01	0.01	0.02	0.03	0.11	0.32	**0.30**	0.10	0.05	0.04	0.03	0.02	1782928
28–30	0.00	0.00	0.00	0.00	0.00	0.00	0.00	0.00	0.00	0.00	0.01	0.02	0.08	0.30	**0.30**	0.11	0.06	0.04	0.03	1024994
30–32	0.00	0.00	0.00	0.00	0.00	0.00	0.00	0.00	0.00	0.00	0.00	0.00	0.01	0.07	0.28	**0.29**	0.11	0.06	0.05	495490
32–34	0.00	0.00	0.00	0.00	0.00	0.00	0.00	0.00	0.00	0.00	0.00	0.00	0.00	0.01	0.06	0.26	**0.28**	0.12	0.07	221965
34–36	0.00	0.00	0.00	0.00	0.00	0.00	0.00	0.00	0.00	0.00	0.00	0.00	0.00	0.00	0.01	0.06	0.25	**0.28**	0.12	95760
>36	0.00	0.00	0.00	0.00	0.00	0.00	0.00	0.00	0.00	0.00	0.00	0.00	0.00	0.00	0.00	0.01	0.05	0.28	**0.55**	47794
n	4641644	1272584	1570363	1922163	2279418	2605791	2892009	3114392	3276134	3341441	3238901	2873505	2198716	1374145	723786	343563	157760	65240	26203	37917758

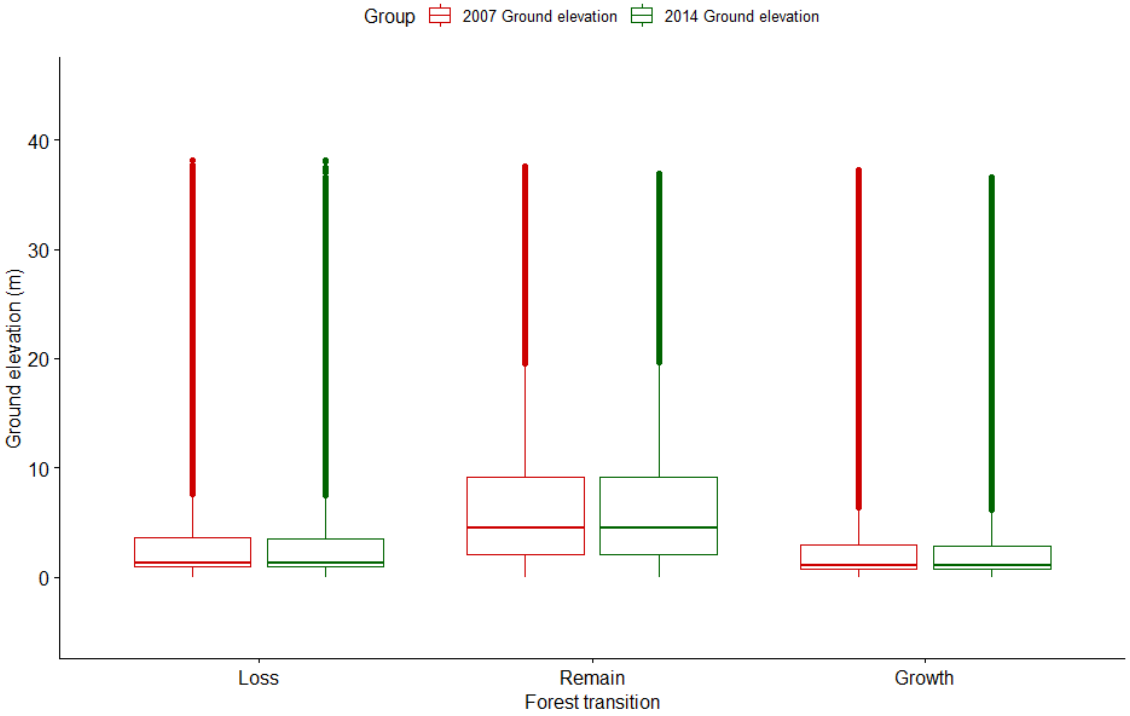

Figure 6. Comparison of ground elevation from 2007 and 2014 between the forest transition classes.

4. Discussion

Between 2007 and 2015, we quantified widespread forest loss along two coastal counties in Delaware. Forest losses were concentrated in the Delaware Bay estuary's southern, more coastal watersheds and negatively correlated with watershed drainage density. Over this short time, the forest loss is consistent with rapid marsh migration, likely driven by a series of episodic events exacerbated by climate change and gradual sea-level rise. In the following discussion, we provide further insight into the results and limitations of this study.

4.1. Classification and Change Map

Coastal ecosystems are challenging to monitor using remote sensing as they are highly dynamic and heterogeneous landscapes. However, the increased availability of data with high spatial and temporal resolution coupled with machine learning classification algorithms could assist in monitoring coastal ecosystem change. This study is one of the few that quantify recent upland forest loss due to marsh migration in Delaware Bay using high-resolution Lidar and imagery. Our classification and subsequent post-classification analysis mapped recent forest loss likely due to marsh migration. Although the user accuracy of forest loss derived from the change map was relatively inaccurate (~49%), the estimated area was "error-adjusted" to reflect the classification error within a confidence interval. While this method is considered a best practice for quantifying post-classification accuracy, many studies leave out the erroneous area attributed to classification error. Overlooking these errors could lead to dramatic differences in numerical models that utilize land change estimates (e.g., carbon flux, carbon storage, biomass loss) [44].

The classification errors accompanying forest change (i.e., forest loss, forest growth) may be attributable to the species composition in the ecotone between the upland forest and the marsh platform. This ecotone is primarily compromised of *P. australis*. These invasive reeds are tall, typically between 2 to 5 m, have a high NDVI value, and are known to colonize rapidly, which we speculate may be easily misclassified as forest in 2009 or 2015 forest/non-forest maps, leading to the errors in the mapping of forest loss and forest growth. The sources of misclassification would be better interpreted with ground

truth landcover reference data. However, ground-truth samples were not available for the periods of our study.

4.2. Landscape Change Analysis

We found that watersheds with higher drainage densities are less likely to experience forest dieback than subregions with lower drainage densities. We were surprised by the negative drainage density coefficient, but this finding is consistent with the results by White et al. (2021), which also found a significant negative coefficient for drainage density when evaluating the predictive power for freshwater forested wetland loss in HUC-4 subregions in the North American coastal plain. While other work has shown that increased connectivity to saline water bodies can drive the salinization and subsequent deforestation of freshwater habitats [27,51,52], we suspect that improper drainage from historic tidal impoundments in our study area may be contributing to upland dieback compared to other regions that may have better drainage networks.

The current tidal impoundments in Delaware serve as a habitat for waterfowl and recreational areas. Yet, these impoundments may have been breached during intense storms, contributing to the rapid conversion from forest to marsh. Inundation from storm surges in impounded areas may not be able to recede as fast as areas that have tidal access, leading to more significant forest dieback [53]. More research is needed to address how historic and current management of these impoundments will affect future marsh migration routes [53].

Ground elevation is a principal determinant of the forest–marsh boundary and its movement with SLR [52,53]. Although we did not find average watershed elevation to be a significant predictor of increased forest loss, we found that ground elevation decreased in areas that experienced forest dieback from 2007 to 2014, suggesting that pulses of inundation from episodic events may be causing root breakdown and ground subsidence, reflected in overall lower ground elevations. This finding agrees with much of the marsh migration literature, which suggests that trees in lower elevations are likely to be converted to marsh first, whereas trees in higher elevations may be able to persist as higher elevations limit the reaches of inundation [7,11,52,54,55].

Increased inundation inland, whether from gradual SLR or episodic events, changes the ecosystem function of forested habitats, which may manifest in vertical forest structure changes. Forest height and the variability in height may provide early evidence of forest seral stage or disturbance to the vegetation [30,56]. Our results show that average canopy height decreased in areas of forest loss over our study period, whereas in regions classified as stable forest and growth, canopy height increased, highlighting the potential of Lidar to provide important information on structural changes attributed to forest retreat before mortality.

Additionally, we can explore particular forest characteristics that may be more susceptible or resilient to marsh migration using data from Lidar. For example, we found that, on average, taller trees (>16 m) do not experience as much dieback as trees that are shorter (<12 m). We speculate that taller forests with more established root systems may allow for enhanced resiliency as deeper roots may access the fresh groundwater from deeper depths [57]. In contrast, shorter forest stands with shallower root systems may be more susceptible to salt stress due to increased exposure to tidal inundation or saltwater intrusion in the groundwater. Our findings are supported by Krauss et al. 2009 [58], who found reductions in freshwater forest height and basal area of areas impacted by saltwater intrusion. Further research is required to determine forest resiliency in response to episodic events of inundation and increased saltwater intrusion.

We also characterized canopy dynamics using a height transition matrix, and while we found that taller height classes tended to remain stable, we identified that all height classes had at least a 7% chance of converting to the shortest height class (< 2 m), indicating a possible disturbance that affected all height classes. This perturbation may have resulted

from prolonged edaphic stress on the forest, which could have resulted in widespread canopy thinning consistent with the effects of marsh migration.

Our transition matrix displays a mortality rate (inferred by height losses) of ~1% per year, which is consistent with estimations of mortality from the United States Forest Service (USFS) of approximately 1–2% [59]. However, the USFS rate includes mortality by harvesting and it is unclear how this mortality rate may extend to coastal forest dieback associated with the effects of accelerated SLR [60].

While Lidar can be a powerful tool to map canopy height over broad scales, validating Lidar-derived height changes can be challenging. Both Lidar acquisitions had a vertical accuracy within 18.5 cm, as defined by the National Digital Elevation Program (NDEP) [61], but we did not have any field height measurements to validate Lidar-derived height changes during our study period. Additionally, the Lidar used for our analysis had low point densities, which could have led to height errors due to points not reaching the ground. Therefore, future efforts should use higher point density Lidar to monitor structural changes through time.

We suspect that regime shifts in the understory could have occurred during our study period (invisible migration, [62]); however, we did not quantify changes to vegetation under the canopy. Additionally, changes to the forest composition, namely, invasions of *P. australis*, could be early signals of marsh migration as *P. australis* is often the first to colonize and can colonize in the understory [8]. As such, future studies using higher resolution Lidar may assist in detecting changes to the understory that are typically limited by canopy cover.

4.3. Drivers for Forest Loss–Episodic Events

The timing and spatial distribution of forest dieback within the estuary suggest that forest mortality reflects the effects of rapid marsh migration following a series of episodic events. Sea level increased by approximately 2.5 cm over our study period (9 years), which is lower than the present rate of SLR (3.76 ± 0.43 mm/year, [63]), leading us to investigate additional drivers that may have caused rapid rates of marsh migration [63].

Over our study period, there were four major coastal storms, here defined as tropical cyclones that were within 30 km of the Delaware coast, categorized based on the Saffir-Simpson Hurricane Wind Scale (i.e., Tropical storm Hanna, 2011; Hurricane Irene, 2011; Hurricane Sandy, 2012; Tropical storm Andrea, 2013). Each of these storms could have caused prolonged flooding, windthrow, and saltwater intrusion to the groundwater, all of which may have contributed to the forest mortality (Table 6) [64]. These hydrologically connected areas are low-lying with shallow groundwater depths, making them, particularly at risk for saltwater intrusion [52,65].

Table 6. List of the major storms that occurred near our study area between 2007 and 2015 with their associated wind speed and category when the storm made landfall.

Hurricane Name	Date	Landfall Wind Speed (Knots)	Category (during Landfall)
Hanna	September 2008	45	Tropical storm
Irene	August 2011	65	Category 1 hurricane
Sandy	October 2012	70	Category 1 hurricane
Andrea	June 2013	45	Tropical storm

Another consideration to be investigated is the effect of drought on coastal tree mortality. Drought conditions can intensify the impacts of the gradual sea-level rise as the availability of fresh groundwater in areas with active marsh transgression is essential for forest stands to cope with salinity pulses [7,24,54,65]. However, if fresh groundwater is limited (e.g., drought-induced), salt-stressed forested regions will begin to convert to marsh [58]. Additionally, severe droughts can cause increased saltwater intrusion into the groundwater because the lack of precipitation allows the salt pulse from the tides to persist,

whereas, with regular rainfall events, those salt pulses associated with the tides tend to get diluted [24]. During prolonged drought events, especially during the growing season when temperatures are hot and evapotranspiration by the vegetation is highest, groundwater can become hypersaline and result in pulses of tree mortality [54].

A considerable drought occurred in the mid-Atlantic in the summer of 2011. The Palmer Drought Severity Index (PDSI) for the study area indicated extreme drought conditions with values between −4.0 to −4.70 during the growing season [66]. We suggest that this severe drought, followed by Hurricane Irene in 2011, with almost a direct hit on the Delaware coast, could have been the main driver for the forest loss and subsequent shift in habitat ranges during our study period. This finding is consistent with previous work during the same time interval in the Chesapeake Bay and Albemarle-Pamlico Estuaries [7,65].

5. Conclusions and Future Directions

This study used publicly available Lidar and NAIP imagery fusion to detect forest losses related to recent marsh migration in two counties along the Delaware Bay Estuary. Although our analysis showed changes in canopy height, our Lidar point density was low, and future efforts to monitor structural changes through time should use the highest point density that is practical and affordable. With state and federal funding for routine airborne Lidar data acquisitions becoming more common, Lidar can be a powerful tool for natural resource managers to map potential marsh conservation corridors as the effects of accelerated sea-level rise persist. In addition, Lidar has the ability to map the upland vegetation's three-dimensional vertical structure, which may enable early detection of initial landscape-level changes associated with sea-level rise and coastal storms ahead of widespread forest dieback.

As policy moves toward expanding coastal wetland restoration to carbon markets and state climate action plans, we first need to determine if, where, and how tidal marshes are expanding into the upland forest to cope with accelerated SLR. Efforts to map marsh migration and upland forest retreat need to consider the effects of SLR while also accounting for extreme events (i.e., hurricanes, drought) as they are inherently linked to global climate change and, as we have shown in this study, may result in rapid marsh migration and extensive forest dieback on sub-decadal timescales.

Author Contributions: Conceptualization, E.B.P. and R.D.; methodology, E.B.P.; formal analysis, E.B.P. and R.D.; resources, K.A.S.L.; original draft writing and preparation, E.B.P.; draft review and editing, R.D. and K.A.S.L.; supervision, R.D. and K.A.S.L. All authors have read and agreed to the published version of the manuscript.

Funding: This research was supported by funding through the Margaret A. Davidson Graduate Research Fellowship through the National Oceanic and Atmospheric Administration (NOAA).

Data Availability Statement: The datasets used in this study were publicly available, and citations for the NAIP and Lidar are listed below. NAIP Digital Ortho Photo Image, Publication date: 20150925, USDA-FSA-APFO Aerial Photography Field Office. NAIP Digital Ortho Photo Image, Publication date: 20091113, USDA-FSA-APFO Aerial Photography Field Office. OCM Partners: 2022: 2014 USGS CMGP Lidar: Sandy Restoration (Delaware and Maryland) from 2010-06-15 to 2010-08-15. NOAA National Centers for Environmental Information, https://www.fisheries.noaa.gov/inport/item/49662. OCM Partners: 2022: 2007 Delaware Coastal Programs Lidar: Kent and New Castle Counties from 2010-06-15 to 2010-08-15. NOAA National Centers for Environmental Information, https://www.fisheries.noaa.gov/inport/item/49660.

Acknowledgments: We thank George Halley and Anya Schneider at Sanborn Map Company Inc. for pertinent Lidar acquisition details and Johannes Krause from Florida International University for constructive feedback that significantly improved this manuscript.

Conflicts of Interest: The authors declare no conflict of interest.

References

1. Mcleod, E.; Chmura, G.L.; Bouillon, S.; Salm, R.; Björk, M.; Duarte, C.M.; Lovelock, C.E.; Schlesinger, W.H.; Silliman, B.R. A Blueprint for Blue Carbon: Toward an Improved Understanding of the Role of Vegetated Coastal Habitats in Sequestering CO_2. *Front. Ecol. Environ.* **2011**, *9*, 552–560. [CrossRef]
2. Gedan, K.B.; Silliman, B.R.; Bertness, M.D. Centuries of Human-Driven Change in Salt Marsh Ecosystems. *Ann. Rev. Mar. Sci.* **2009**, *1*, 117–141. [CrossRef] [PubMed]
3. Sallenger, A.H.; Doran, K.S.; Howd, P.A. Hotspot of Accelerated Sea-Level Rise on the Atlantic Coast of North America. *Nat. Clim. Chang.* **2012**, *2*, 884–888. [CrossRef]
4. Smart, L.S.; Taillie, P.J.; Poulter, B.; Vukomanovic, J.; Singh, K.K.; Swenson, J.J.; Mitasova, H.; Smith, J.W.; Meentemeyer, R.K. Aboveground Carbon Loss Associated with the Spread of Ghost Forests as Sea Levels Rise. *Environ. Res. Lett.* **2020**, *15*, 104028. [CrossRef]
5. Bertness, M.D.; Ellison, A.M. Determinants of Pattern in a New England Salt Marsh Plant Community. *Ecol. Monogr.* **1987**, *57*, 129–147. [CrossRef]
6. Kirwan, M.L.; Temmerman, S.; Skeehan, E.E.; Guntenspergen, G.R.; Fagherazzi, S. Overestimation of Marsh Vulnerability to Sea Level Rise. *Nat. Clim. Chang.* **2016**, *6*, 253–260. [CrossRef]
7. Gedan, K.B.; Epanchin-Niell, R.; Qi, M. Rapid Land Cover Change in a Submerging Coastal County. *Wetlands* **2020**, *40*, 1717–1728. [CrossRef]
8. Shaw, P.; Jobe, J.; Gedan, K.B. Environmental Limits on the Spread of Invasive Phragmites Australis into Upland Forests with Marine Transgression. *Estuaries Coasts* **2022**, *45*, 539–550. [CrossRef]
9. Brinson, M.M.; Christian, R.R.; Blum, L.K. Multiple States in the Sea-Level Induced Transition from Terrestrial Forest to Estuary. *Estuaries* **1995**, *18*, 648. [CrossRef]
10. Kirwan, M.L.; Megonigal, J.P. Tidal Wetland Stability in the Face of Human Impacts and Sea-Level Rise. *Nature* **2013**, *504*, 53–60. [CrossRef]
11. Fagherazzi, S.; Anisfeld, S.C.; Blum, L.K.; Long, E.V.; Feagin, R.A.; Fernandes, A.; Kearney, W.S.; Williams, K. Sea Level Rise and the Dynamics of the Marsh-Upland Boundary. *Front. Environ. Sci.* **2019**, *7*, 25. [CrossRef]
12. Kirwan, M.L.; Gedan, K.B. Sea-Level Driven Land Conversion and the Formation of Ghost Forests. *Nat. Clim. Chang.* **2019**, *9*, 450–457. [CrossRef]
13. Raabe, E.A.; Stumpf, R.P. Expansion of Tidal Marsh in Response to Sea-Level Rise: Gulf Coast of Florida, USA. *Estuaries Coasts* **2016**, *39*, 145–157. [CrossRef]
14. Williams, K.; Ewel, K.C.; Stumpf, R.P.; Putz, F.E.; Workman, T.W. Sea-Level Rise and Coastal Forest Retreat on the West Coast of Florida, USA. *Ecology* **1999**, *80*, 2045–2063. [CrossRef]
15. Poulter, B. *Interactions between Landscape Disturbance and Gradual Environmental Change: Plant Community Migration in Response to Fire and Sea Level Rise*; Duke University: Durham, NC, USA, 2005.
16. Robichaud, A.; Bégin, Y. The Effects of Storms and Sea-Level Rise on a Coastal Forest Margin in New Brunswick, Eastern Canada. *J. Coast. Res.* **1997**, *13*, 429–439.
17. Webster, P.J.; Holland, G.J.; Curry, J.A.; Chang, H.-R. Changes in Tropical Cyclone Number, Duration, and Intensity in a Warming Environment. *Science* **2005**, *309*, 1844–1846. [CrossRef]
18. Kozlowski, T.T. (Ed.) Flooding and Plant Growth. In *Physiological Ecology*; Academic Press: Orlando, FL, USA, 1984; ISBN 978-0-12-424120-6.
19. Kozlowski, T.T. Responses of Woody Plants to Flooding and Salinity. *Tree Physiol.* **1997**, *17*, 490. [CrossRef]
20. Kozlowski, T.T. Physiological-Ecological Impacts of Flooding on Riparian Forest Ecosystems. *Wetlands* **2002**, *22*, 550–561. [CrossRef]
21. Blood, E.R.; Anderson, P.; Smith, P.A.; Nybro, C.; Ginsberg, K.A. Effects of Hurricane Hugo on Coastal Soil Solution Chemistry in South Carolina. *Biotropica* **1991**, *23*, 348. [CrossRef]
22. Merry, K.; Bettinger, P.; Hepinstall, J. Physical and Biological Responses of Forests to Tropical Cyclones Affecting the United States Atlantic Ocean and Gulf of Mexico Coasts. *Am. J. Environ. Sci.* **2009**, *5*, 16–32. [CrossRef]
23. Kearney, W.S.; Fernandes, A.; Fagherazzi, S. Sea-Level Rise and Storm Surges Structure Coastal Forests into Persistence and Regeneration Niches. *PLoS ONE* **2019**, *14*, e0215977. [CrossRef] [PubMed]
24. Tully, K.; Gedan, K.; Epanchin-Niell, R.; Strong, A.; Bernhardt, E.S.; BenDor, T.; Mitchell, M.; Kominoski, J.; Jordan, T.E.; Neubauer, S.C.; et al. The Invisible Flood: The Chemistry, Ecology, and Social Implications of Coastal Saltwater Intrusion. *BioScience* **2019**, *69*, 368–378. [CrossRef]
25. Schuerch, M.; Spencer, T.; Temmerman, S.; Kirwan, M.L.; Wolff, C.; Lincke, D.; McOwen, C.J.; Pickering, M.D.; Reef, R.; Vafeidis, A.T.; et al. Future Response of Global Coastal Wetlands to Sea-Level Rise. *Nature* **2018**, *561*, 231–234. [CrossRef] [PubMed]
26. Törnqvist, T.E.; Cahoon, D.R.; Morris, J.T.; Day, J.W. Coastal Wetland Resilience, Accelerated Sea-Level Rise, and the Importance of Timescale. *AGU Adv.* **2021**, *2*, e2020AV000334. [CrossRef]
27. White, E.E.; Ury, E.A.; Bernhardt, E.S.; Yang, X. Climate Change Driving Widespread Loss of Coastal Forested Wetlands Throughout the North American Coastal Plain. *Ecosystems* **2021**, *25*, 812–827. [CrossRef]
28. Magolan, J.L.; Halls, J.N. A Multi-Decadal Investigation of Tidal Creek Wetland Changes, Water Level Rise, and Ghost Forests. *Remote Sens.* **2020**, *12*, 1141. [CrossRef]

29. Smith, J.A.M. The Role of Phragmites Australis in Mediating Inland Salt Marsh Migration in a Mid-Atlantic Estuary. *PLoS ONE* **2013**, *8*, e65091. [CrossRef]
30. Dubayah, R.; Blaire, J.B.; Bufton, J.L.; Clark, D.B.; Jaja, J.; Knox, R.G.; Luthcke, S.P.; Weishampel, J.F. The Vegetation Canopy Lidar Mission. In Proceedings of the Land Satellite Information in the Next 1 Decade II: Sources and Applications, Bethesda, MD, USA, 20 March 1997; pp. 100–112.
31. Lovell, J.L.; Jupp, D.L.B.; Newnham, G.J.; Coops, N.C.; Culvenor, D.S. Simulation Study for Finding Optimal Lidar Acquisition Parameters for Forest Height Retrieval. *For. Ecol. Manag.* **2005**, *214*, 398–412. [CrossRef]
32. Zurqani, H.A.; Post, C.J.; Mikhailova, E.A.; Cope, M.P.; Allen, J.S.; Lytle, B.A. Evaluating the Integrity of Forested Riparian Buffers over a Large Area Using LiDAR Data and Google Earth Engine. *Sci. Rep.* **2020**, *10*, 14096. [CrossRef]
33. Anderson, M.G.; Clark, L.; Ferree, C.E.; Jospe, A.; Sheldon, A.O.; Weaver, K.J. *The Northeast Habitat Guides: A Companion to the Terrestrial and Aquatic Habitat Maps*; The Nature Conservancy: Boston, MA, USA, 2013.
34. Sacatelli, R.; Lathrop, R.; Kaplan, M.B. *Impacts of Climate Change on Coastal Forests in the Northeast US*; Rutgers University: New Brunswick, NJ, USA, 2020.
35. O'neil-Dunne, J. *CMS: LiDAR-Derived Tree Canopy Cover for Pennsylvania, USA, 2008*; ORNL DAAC: Oak Ridge, TN, USA, 2016.
36. Roussel, J.-R.; Auty, D.; Coops, N.C.; Tompalski, P.; Goodbody, T.R.H.; Meador, A.S.; Bourdon, J.-F.; de Boissieu, F.; Achim, A. LidR: An R Package for Analysis of Airborne Laser Scanning (ALS) Data. *Remote Sens. Environ.* **2020**, *251*, 112061. [CrossRef]
37. Torresani, M.; Rocchini, D.; Sonnenschein, R.; Zebisch, M.; Hauffe, H.C.; Heym, M.; Pretzsch, H.; Tonon, G. Height Variation Hypothesis: A New Approach for Estimating Forest Species Diversity with CHM LiDAR Data. *Ecol. Indic.* **2020**, *117*, 106520. [CrossRef]
38. EarthExplorer. Available online: https://earthexplorer.usgs.gov/ (accessed on 11 April 2022).
39. Smith, A.B. U.S. Billion-Dollar Weather and Climate Disasters, 1980-Present (NCEI Accession 0209268) 2020. Available online: https://www.ncei.noaa.gov/access/billions/ (accessed on 14 May 2022).
40. Liaw, A.; Wiener, M. Classification and Regression by RandomForest. *R J.* **2002**, *2*, 18–22.
41. Kuhn, M.; Wing, J.; Weston, S.; Williams, A.; Keefer, C.; Engelhardt, A.; Cooper, T.; Mayer, Z.; Kenkel, B.; R Core Team; et al. Caret: Classification and Regression Training. Available online: https://CRAN.R-project.org/ (accessed on 19 July 2022).
42. Belgiu, M.; Drăguţ, L. Random Forest in Remote Sensing: A Review of Applications and Future Directions. *ISPRS J. Photogramm. Remote Sens.* **2016**, *114*, 24–31. [CrossRef]
43. Breiman, L. Random Forests. *Mach. Learn.* **2001**, *45*, 5–32. [CrossRef]
44. Olofsson, P.; Foody, G.M.; Stehman, S.V.; Woodcock, C.E. Making Better Use of Accuracy Data in Land Change Studies: Estimating Accuracy and Area and Quantifying Uncertainty Using Stratified Estimation. *Remote Sens. Environ.* **2013**, *129*, 122–131. [CrossRef]
45. Stehman, S.V.; Sohl, T.L.; Loveland, T.R. An Evaluation of Sampling Strategies to Improve Precision of Estimates of Gross Change in Land Use and Land Cover. *Int. J. Remote Sens.* **2005**, *26*, 4941–4957. [CrossRef]
46. Card, D. Using Known Map Category Marginal Frequencies to Improve Estimates of Thematic Map Accuracy. *Photogramm. Eng. Remote Sens.* **1982**, *48*, 431–439.
47. FirstMap. Available online: https://firstmap-delaware.opendata.arcgis.com/datasets/?group_ids=53397d2551134caa8e9abb62ff30df12 (accessed on 1 June 2022).
48. Kellner, J.R.; Clark, D.B.; Hubbell, S.P. Pervasive Canopy Dynamics Produce Short-Term Stability in a Tropical Rain Forest Landscape. *Ecol. Lett.* **2009**, *12*, 155–164. [CrossRef]
49. Dubayah, R.O.; Sheldon, S.L.; Clark, D.B.; Hofton, M.A.; Blair, J.B.; Hurtt, G.C.; Chazdon, R.L. Estimation of Tropical Forest Height and Biomass Dynamics Using Lidar Remote Sensing at La Selva, Costa Rica: Forest Dynamics Using Lidar. *J. Geophys. Res.* **2010**, *115*. [CrossRef]
50. O'neil-Dunne, J. *CMS: LiDAR-Derived Tree Canopy Cover for States in the Northeast USA*; ORNL DAAC: Oak Ridge, TN, USA, 2019.
51. Herbert, E.R.; Boon, P.; Burgin, A.J.; Neubauer, S.C.; Franklin, R.B.; Ardón, M.; Hopfensperger, K.N.; Lamers, L.P.M.; Gell, P. A Global Perspective on Wetland Salinization: Ecological Consequences of a Growing Threat to Freshwater Wetlands. *Ecosphere* **2015**, *6*, 1–43. [CrossRef]
52. Bhattachan, A.; Emanuel, R.E.; Ardón, M.; Bernhardt, E.S.; Anderson, S.M.; Stillwagon, M.G.; Ury, E.A.; BenDor, T.K.; Wright, J.P. Evaluating the Effects of Land-Use Change and Future Climate Change on Vulnerability of Coastal Landscapes to Saltwater Intrusion. *Elem. Sci. Anthropocene* **2018**, *6*, 62. [CrossRef]
53. Smith, J.A.M.; Hafner, S.F.; Niles, L.J. The Impact of Past Management Practices on Tidal Marsh Resilience to Sea Level Rise in the Delaware Estuary. *Ocean Coast. Manag.* **2017**, *149*, 33–41. [CrossRef]
54. Williams, K.; MacDonald, M. Interactions of Storm, Drought, and Sea-Level Rise on Coastal Forest: A Case Study. *J. Coast. Res.* **2003**, *19*, 7.
55. Anderson, S.M.; Ury, E.A.; Taillie, P.J.; Ungberg, E.A.; Moorman, C.E.; Poulter, B.; Ardón, M.; Bernhardt, E.S.; Wright, J.P. Salinity Thresholds for Understory Plants in Coastal Wetlands. *Plant Ecol.* **2022**, *223*, 323–337. [CrossRef]
56. Goetz, S.; Dubayah, R. Advances in Remote Sensing Technology and Implications for Measuring and Monitoring Forest Carbon Stocks and Change. *Carbon Manag.* **2011**, *2*, 231–244. [CrossRef]
57. Brando, P. Tree Height Matters. *Nat. Geosci.* **2018**, *11*, 390–391. [CrossRef]
58. Krauss, K.W.; Duberstein, J.A. Sapflow and Water Use of Freshwater Wetland Trees Exposed to Saltwater Incursion in a Tidally Influenced South Carolina Watershed. *Can. J. For. Res.* **2010**, *40*, 525–535. [CrossRef]

59. Oswalt, S.N.; Smith, W.B.; Miles, P.D.; Pugh, S.A. *Forest Resources of the United States, 2017: A Technical Document Supporting the Forest Service 2020 RPA Assessment*; U.S. Department of Agriculture, Forest Service: Washington, DC, USA, 2019; p. WO-GTR-97.
60. Clark, J.S. Coastal Forest Tree Populations in a Changing Environment, Southeastern Long Island, New York. *Ecol. Monographs* **1986**, *56*, 259–277. [CrossRef]
61. Osborn, K.; List, J.; Gesch, D.B.; Crowe, J.; Merrill, G.; Constance, E.; Mauck, J.; Lund, C.; Caruso, V.; Kosovich, J. *National Digital Elevation Program (NDEP)*; American Society for Photogrammetry and Remote Sensing: Bethesda, MD, USA, 2001; pp. 83–120.
62. Anisfeld, S.C.; Kemp, A.C.; O'Connell, J. Salt Marsh Migration into Lawns Revealed by a Novel Sediment-Based Approach. *Estuaries Coasts* **2019**, *42*, 1419–1429. [CrossRef]
63. Station Home Page-NOAA Tides & Currents. Available online: https://tidesandcurrents.noaa.gov/stationhome.html?id=8537121 (accessed on 11 April 2022).
64. Historical Hurricane Tracks. Available online: https://coast.noaa.gov/hurricanes/#map=4/32/-80 (accessed on 6 June 2022).
65. Ury, E.A.; Yang, X.; Wright, J.P.; Bernhardt, E.S. Rapid Deforestation of a Coastal Landscape Driven by Sea-level Rise and Extreme Events. *Ecol. Appl.* **2021**, *31*, e02339. [CrossRef]
66. Climate at a Glance | National Centers for Environmental Information (NCEI). Available online: https://www.ncdc.noaa.gov/cag/divisional/time-series/0702/pdsi/all/3/2007-2015?base_prd=true&begbaseyear=1901&endbaseyear=2000 (accessed on 14 April 2022).